7e JOURNEES DE L'HYDRODYNAMIQUE

MARSEILLE - 8, 9, 10 MARS 1999

FOURIER-KOCHIN REPRESENTATION OF FARFIELD STEADY SHIP WAVES

NOBLESSE F.*, YANG C.**, LÖHNER R.**, HENDRIX D.*

* David Taylor Model Basin, NSWC-CD
9500 MacArthur Blvd
West Bethesda, MD 20817-5700, USA
Tel: 301 227 7018
Fax: 301 227 4607
e-mail: noblesse@dt.navy.mil

** Institute for Computational Science and Informatics
George Mason University
Fairfax, VA 22030-4444, USA
Tel: 703 993 4077
Fax: 703 993 4064
e-mail: cyang@gmu.edu

Summary

The Fourier-Kochin representation of steady ship waves is used to extend nearfield steady ship waves into the farfield. The coupling of nearfield and farfield ship waves using the Fourier-Kochin theory is based on two main fundamental theoretical results. These fundamental results are summarized, and the Fourier-Kochin representation of farfield steady ship waves is given. The Fourier-Kochin flow representation is verified by considering the waves generated by a submerged point source. An illustrative application to the farfield extension of the nearfield flow about the Wigley hull — determined using a fully nonlinear calculation method based on the Euler equations — is also presented.

Résumé

La représentation de Fourier-Kochin de l'écoulement permanent autour d'une carène de navire est appliquée au prolongement lointain d'un écoulement proche. Le couplage entre un écoulement proche et la représentation de Fourier-Kochin de l'écoulement potentiel linéaire lointain est fondé sur deux résultats théoriques fondamentaux. Ces résultats fondamentaux sont résumés, et la représentation de Fourier-Kochin du champ de vagues lointain est présentée. La représentation de Fourier-Kochin est vérifiée par l'étude du champ de vagues créé par une source ponctuelle submergée. Une application au prolongement lointain de l'écoulement proche — calculé au moyen d'une méthode de résolution numérique des équations d'Euler — autour de la coque de Wigley est aussi présentée.

Introduction

The Fourier-Kochin theory of steady and time-harmonic ship waves expounded in *Noblesse et al. (1997,1999)* is applied to the coupling of nearfield and farfield *steady* ship waves. More precisely, the Fourier-Kochin representation of ship waves is used to extend nonlinear nearfield steady ship waves into the far field. The nearfield ship waves are determined here using the fully nonlinear calculation method, based on the Euler flow equations, of *Yang and Löhner (1998)*.

The coupling of nearfield and farfield ship waves using the Fourier-Kochin theory is based on two main fundamental theoretical results. These fundamental results are first summarized. Next, the Fourier-Kochin representation of farfield steady ship waves is given. The waves due to a submerged point source are then considered for purposes of validation. Finally, an illustrative application to the farfield extension of the nearfield flow about the Wigley hull is presented.

Fourier-Kochin theory of steady and time-harmonic ship waves

The Fourier-Kochin theory of steady and time-harmonic ship waves is based on two fundamental theoretical results. These important theoretical results are now summarized.

One result, given in *Noblesse et al. (1997)*, is a new boundary-integral representation of steady and time-harmonic free-surface potential flows with forward speed. This boundary-integral representation defines the velocity field $\nabla\phi$ in a potential flow ***explicitly*** in terms of the velocity distribution (u, v, w) at a boundary surface Σ. Thus, this flow representation does not involve the potential ϕ at Σ — unlike the usual Green identity which expresses ϕ within a flow domain in terms of boundary values of the potential ϕ and its normal derivative $\partial\phi/\partial n$ — and defines the velocity field $\nabla\phi$ directly, instead of via numerical differentiation of ϕ. The new flow representation can be used to extend a given nearfield flow (determined using any nearfield flow solver, including solvers based on finite differences or Rankine singularities) into the far field, and to couple a viscous nearfield flow — for which a velocity potential cannot be defined — and a farfield linear potential-flow representation.

Another result, given in *Noblesse et al. (1999)*, is a new mathematical representation of steady and time-harmonic free-surface flows with forward speed generated by ***arbitrary*** distributions of singularities (e.g., sources and dipoles) over (flat or curved) hull-panels or waterline-segments. Such flows are called *super Green functions* because of the similarity and difference with ordinary Green functions, which are associated with a *point* source instead of a ***distribution*** of singularities. The mathematical representation of super Green functions given in *Noblesse et al. (1999)* is valid for a broad class of waves in *generic* dispersive media. This representation of generic super Green functions provides a useful formal decomposition of nearfield free-surface flows (and other dispersive waves) into a nonoscillatory *local component*, which decays rapidly and is significant only in the near field, and a *wave component* which fully accounts for the waves in the near field (as well as in the far field where the local component is negligible). The expression for the wave component, given by single Fourier integrals along the curves (called dispersion curves) defined by the dispersion relation, is especially simple and is well suited for accurate and efficient numerical evaluation.

This Fourier representation of the wave component in the mathematical representation of generic super Green functions and the boundary-integral flow representation given in *Noblesse et al. (1997)* are used in this study to determine the farfield steady ship waves generated by a prescribed velocity distribution at a boundary surface, and to extend nonlinear steady ship waves predicted by a nearfield calculation method into the far field. The *nearfield wave drag* determined via integration of the hull pressure and the *farfield wave drag* obtained from the Havelock formula for the radiated wave energy are in relatively fair agreement.

Farfield extension of nearfield steady ship waves

Consider a ship advancing along a straight path, with constant speed $\mathcal{U}$, in calm water of effectively infinite depth and lateral extent. The flow is observed from a Cartesian system of coordinates moving with the ship. The X axis is taken along the path of the ship and points toward the ship bow; thus, the ship advances in the direction of the *positive* X axis. The Z axis is vertical and points upward, and the mean free surface is chosen as the plane $Z=0$. The flow appears steady in the translating system of coordinates, and consists of the disturbance flow due to the ship superimposed on a uniform stream opposing the ship's forward speed. The components of the *disturbance* velocity along the (X,Y,Z) axes are denoted (U,V,W). Thus, the *total* velocity is given by $(U-\mathcal{U},V,W)$. Nondimensional coordinates and velocities are defined in terms of a characteristic length L (typically the ship length) and the ship speed $\mathcal{U}$ as

$$(x,y,z) = (X,Y,Z)/L \qquad\qquad (u,v,w) = (U,V,W)/\mathcal{U}$$

A geometrical surface Σ surrounding the ship is considered. The intersection curve between the surface Σ and the mean free-surface plane $z=0$ is denoted Γ. The unit vector $\vec{n} = (n^x, n^y, n^z)$ normal to the surface Σ points *outside* Σ. The unit vector $\vec{t} = (t^x, t^y, 0)$ tangent to the curve Γ is oriented *clockwise*. The flow in the region outside Σ is assumed to be potential and linear; i.e. the classical Kelvin linear boundary condition $\partial u/\partial\xi + 2\nu\, w = 0$ is assumed to hold at the mean free-surface plane $z=0$ outside Γ. Here, ν is defined as

$$\nu = 1/(2F^2) \qquad \text{with} \qquad F = \mathcal{U}/\sqrt{gL}$$

F is the Froude number and g is the acceleration of gravity. The flow in the *outer* linear potential-flow region can then be defined using a boundary-integral representation based on the Green function satisfying the Kelvin boundary condition. The boundary-integral representation given in *Noblesse et al. (1997)* is used here. This boundary-integral representation defines the disturbance velocity $\vec{u}(\vec{\xi})$, at a field point $\vec{\xi} = (\xi,\eta,\zeta \le 0)$ of the linear potential-flow region outside a boundary surface Σ, generated by a given disturbance velocity distribution $\vec{u}_g(\vec{x})$ at $\Sigma\cup\Gamma$ *explicitly* in terms of the velocity distribution $\vec{u}_g$.

The Green function G associated with the Kelvin free-surface boundary condition is given by the sum of a simple-singularity component G^S defined in terms of simple Rankine singularities, and a component G^F that accounts for free-surface effects and is defined by a double Fourier superposition of elementary waves. Thus, the free-surface Green function is expressed in terms of two complementary fundamental solutions of the Laplace equation, namely the simple Rankine singularity $1/r$ and the elementary wave function $\exp[\,kz + i\,(\alpha x + \beta y)\,]$, which are well suited for representing a local flow disturbance and the system of waves generated by a ship, respectively. The velocity field $\vec{u}$ can similarly be expressed as the sum of a simple-singularity component $\vec{u}^S$ given by distributions of simple Rankine singularities over $\Sigma\cup\Gamma$, and a free-surface component $\vec{u}^F$ given by a double Fourier superposition of elementary waves. The Fourier representation of free-surface effects $\vec{u}^F$ can be further decomposed into a wave component $\vec{u}^W$ and a local component $\vec{u}^L$, as shown in *Noblesse et al. (1999)*. Thus, the velocity field $\vec{u}$ can be expressed in terms of the flow decomposition

$$\vec{u} = \vec{u}^W + \vec{u}^L + \vec{u}^S \tag{1}$$

This flow decomposition becomes $\vec{u} \approx \vec{u}^W$ at some distance downstream from the surface Σ, where the local component $\vec{u}^L$ and the simple-singularity component $\vec{u}^S$ are negligible.

The velocity field $\vec{u}(\vec{\xi})$, at a field point $\vec{\xi} = (\xi,\eta,\zeta \le 0)$ of a linear potential-flow region *downstream* from a surface Σ, generated by a given velocity distribution $\vec{u}_g(\vec{x})$ over $\Sigma\cup\Gamma$ is now defined. Only the wave component $\vec{u}^W$ is considered in the present study. Both $\vec{u}$ and $\vec{u}_g$ are *disturbance* velocities.

Fourier-Kochin representation of farfield steady ship waves

At a point $\vec{\xi}$ *behind* the boundary surface Σ, the wave component $\vec{u}^W(\vec{\xi})$ is given by

$$4\pi \begin{Bmatrix} u^W \\ v^W \\ w^W \end{Bmatrix} = \int_{-\infty}^{\infty} \frac{d\beta\, \alpha}{k-\nu}\, \Re e \begin{Bmatrix} \alpha \\ \beta \\ i\,k \end{Bmatrix} S\, e^{\zeta k - i(\xi\alpha+\eta\beta)}$$

The Fourier variable α and the wavenumber $k = \sqrt{\alpha^2+\beta^2}$ are functions of the Fourier variable β given by

$$k(\beta) = \nu + \sqrt{\nu^2+\beta^2} \qquad\qquad \alpha(\beta) = \sqrt{k(\beta)}\,/F \tag{2}$$

These relations ensure that the dispersion relation $F^2\alpha^2 = k$ is satisfied. $S \equiv S(\alpha,\beta)$ is the spectrum function associated with the velocity distribution over $\Sigma\cup\Gamma$. The spectrum function S is defined further on. The wave component $\vec{u}^W$ may be expressed as

$$4\pi \begin{Bmatrix} u^W \\ v^W \\ w^W \end{Bmatrix} \approx \int_{-\beta_c}^{\beta_c} \frac{d\beta\, \alpha}{k-\nu} \begin{Bmatrix} \alpha\,(S_r\cos\varphi + S_i\sin\varphi) \\ \beta\,(S_r\cos\varphi + S_i\sin\varphi) \\ k\,(S_r\sin\varphi - S_i\cos\varphi) \end{Bmatrix} e^{\zeta k - C\beta^4/\beta_c^4}$$

where $\varphi = \xi\,\alpha + \eta\,\beta$, S_r and S_i stand for the real and imaginary parts of the spectrum function S, and β_c and C are positive real constants satisfying the conditions $\beta_c \gg 1$ and $e^{-C} \ll 1$.

The integration range in the foregoing Fourier representation of the wave component can be reduced in half :

$$4\pi \begin{Bmatrix} u^W \\ v^W \\ w^W \end{Bmatrix} \approx \int_{0}^{\beta_c} \frac{d\beta\, \alpha}{k-\nu} \begin{Bmatrix} \alpha\, A^\alpha \\ \beta\, A^\beta \\ k\, A^k \end{Bmatrix} e^{\zeta k - C\beta^4/\beta_c^4} \tag{3a}$$

Here, the functions A^α, A^β, and A^k are defined as

$$\begin{aligned} A^\alpha = {} & [\,(S_r^+ + S_r^-)\cos(\xi\,\alpha) + (S_i^+ + S_i^-)\sin(\xi\,\alpha)\,]\cos(\eta\beta) \\ & + [\,(S_i^+ - S_i^-)\cos(\xi\,\alpha) - (S_r^+ - S_r^-)\sin(\xi\,\alpha)\,]\sin(\eta\,\beta) \end{aligned} \tag{3b}$$

$$\begin{aligned} A^\beta = {} & [\,(S_i^+ + S_i^-)\cos(\xi\,\alpha) - (S_r^+ + S_r^-)\sin(\xi\,\alpha)\,]\sin(\eta\,\beta) \\ & + [\,(S_r^+ - S_r^-)\cos(\xi\,\alpha) + (S_i^+ - S_i^-)\sin(\xi\,\alpha)\,]\cos(\eta\,\beta) \end{aligned} \tag{3c}$$

$$\begin{aligned} A^k = {} & [\,(S_r^+ - S_r^-)\cos(\xi\,\alpha) + (S_i^+ - S_i^-)\sin(\xi\,\alpha)\,]\sin(\eta\,\beta) \\ & - [\,(S_i^+ + S_i^-)\cos(\xi\,\alpha) - (S_r^+ + S_r^-)\sin(\xi\,\alpha)\,]\cos(\eta\,\beta) \end{aligned} \tag{3d}$$

where $S_r^\pm \equiv S_r(\alpha,\pm\beta)$ and $S_i^\pm \equiv S_i(\alpha,\pm\beta)$.

The spectrum function S is given by a distribution of elementary waves $\exp[\,kz + i\,(\alpha x+\beta y)\,]$:

$$S(\alpha,\beta) = \int_\Sigma d\mathcal{A}(\vec{x})\, e^{kz+i(\alpha x+\beta y)} A^\Sigma(\vec{x}) + F^2 \int_\Gamma d\mathcal{L}(\vec{x})\, e^{i(\alpha x+\beta y)} A^\Gamma(\vec{x}) \tag{4a}$$

Here, $d\mathcal{A}(\vec{x})$ and $d\mathcal{L}(\vec{x})$ respectively stand for the differential elements of area and arc length of Σ and Γ at the integration point $\vec{x} = (x,y,z\le 0)$, and the amplitude functions A^Σ and A^Γ are defined in terms of the given boundary velocity distribution $\vec{u}_g$ by

$$A^\Sigma = (n^x u_g + n^y v_g + n^z w_g) + i\,[\,(n^x w_g - n^z u_g)\,\frac{\alpha}{k} - (n^z v_g - n^y w_g)\,\frac{\beta}{k}\,] \tag{4b}$$

$$A^\Gamma = (t^x t^y + \frac{\alpha\beta}{k^2})\,(t^x u_g + t^y v_g) + (t^y)^2(t^y u_g - t^x v_g) = \frac{\alpha\beta}{k^2}\,(t^x u_g + t^y v_g) + t^y u_g \tag{4c}$$

Thus, the farfield waves $\vec{u}^W(\vec{\xi})$ generated by a velocity distribution $\vec{u}_g(\vec{x})$ over a surface $\Sigma \cup \Gamma$ are defined by the Fourier representation (3) where the spectrum function S is given by the distribution of elementary waves (4). The drag $D^W = \rho \mathcal{U}^2 L^2 C^W$ associated with the wave energy transported by the farfield waves (3) can also be determined from the spectrum function S using the Havelock formula

$$C^W = \frac{\nu}{2\pi} \int_{-\beta_c}^{\beta_c} \frac{d\beta\, k}{k - \nu} (S_r^2 + S_i^2)\, e^{-C\beta^4/\beta_c^4} \tag{5}$$

where S_r and S_i are the real and imaginary parts of the spectrum function (4), as already noted.

Verification of Fourier-Kochin flow representation for a submerged point source

For the purpose of verifying the foregoing Fourier-Kochin representation of farfield steady ship waves, the linear free-surface potential flow due to a submerged point source of unit strength, i.e. a Green function, is considered. Briefly, the disturbance velocity generated by the point source is evaluated at a boundary surface Σ that encloses the source. This boundary velocity distribution is then extended outside Σ using the Fourier-Kochin flow representation. The *outer* flow fields — outside Σ — determined *directly*, by using the expressions for the gradient of the Green function summarized in *Ponizy et al. (1994)*, and *reconstructed* via the Fourier-Kochin representation are then compared.

Thus, we now consider the linearized potential flow generated by a point source of unit strength advancing with constant speed $\mathcal{U}$ along a straight path submerged a depth D below the mean free-surface plane $z = 0$. The submergence depth D is taken as the previously-defined characteristic length L. The Froude number F is then given by $F = \mathcal{U}/\sqrt{gD}$. The flow is observed from a moving system of coordinates attached to the source and therefore appears steady. The x axis is chosen parallel to the path of the moving source and points in the direction of motion of the source. The z axis is vertical and points upward. The origin of the system of coordinates is taken in the mean free-surface plane $z = 0$ and above the source, which is then located at $(0, 0, -1)$. The disturbance velocity generated by the source, at a matching boundary surface Σ and in a flow region outside Σ, is evaluated using the integral representations of the gradient of the Green function summarized in *Ponizy et al. (1994)*, as already noted.

For the purpose of verifying that the Fourier-Kochin extension of the velocity distribution generated by the source at a matching boundary surface Σ is independent of Σ, two matching boundary surfaces Σ are actually considered. These matching surfaces are chosen as half spheres, centered at $(0, 0, 0)$, with radii equal to 3 and 4.5, i.e. 3 and 4.5 times the submergence depth of the point source. The velocity distributions (u, v, w) generated by the point source at the *large* and *small* half spheres are depicted in Fig. 1a for a Froude number equal to 1. Fig. 1a shows that the velocity distributions over the two half spheres are different, as one expects.

The spectrum functions S associated with the velocity distributions over the large and small spheres are considered in Fig. 1b, where the left and right columns respectively correspond to the real and imaginary parts S_r and S_i of S. As is indicated in (4a), the spectrum function S associated with a velocity distribution over a matching boundary surface $\Sigma \cup \Gamma$ is given by distributions of elementary waves over the surface Σ and the intersection curve Γ of the surface Σ with the plane $z = 0$. In the present case, Σ and Γ are half spheres and circles centered at the origin $(0, 0, 0)$. The first (top) and second rows in Fig. 1b respectively show the contributions of the surface Σ and of the curve Γ to the spectrum function S. The *surface* and *curve* contributions to S can be seen to be different for the large and small half spheres, in accordance with the fact that the velocity distributions over these two half spheres are not identical (Fig. 1a).

Expressions (3) and (5) show that the farfield waves, and the related wave drag, associated with a velocity distribution over a boundary surface $\Sigma \cup \Gamma$ are determined by the spectrum function S, which is defined by (4) as the *sum* of surface and curve contributions. Thus, if the

Fourier-Kochin extension of the velocity distribution generated by the point source at a matching boundary surface Σ is to be independent of Σ as one expects, the *sum* of the surface and curve contributions to the spectrum function S ought to be the same for the large and small spheres. This expectation can be verified from the third (middle) row in Fig. 1b, which depicts the sum of the surface and curve contributions to the spectrum function (4). Note that in the present case, the imaginary part S_i is null and the real part S_r is nonoscillatory, even though the surface and curve contributions to the spectrum function are oscillatory functions of β.

The fourth row of Fig. 1b shows the surface and curve contributions to the spectrum function S for the large sphere, and the fifth (bottom) row presents the same information for the small sphere. The imaginary parts of the surface and curve contributions to S may be seen to entirely cancel out (the third row of Fig. 1b shows that $S_i = 0$, as was already noted). Significant cancellations occur also between the real parts of the surface and curve contributions to S. These cancellations require accurate numerical evaluation of the spectrum function.

Fig. 1c depicts the wave patterns generated by the submerged point source for two values of the Froude number equal to 1 (left half of Fig. 1c) and 1.25 (right half). The *direct* wave patterns, computed from the expressions for the gradient of the Green function given in *Ponizy et al. (1994)*, and the *reconstructed* Fourier-Kochin patterns are shown side by side. The intersection circle Γ of the matching half sphere Σ with the plane $z = 0$ is shown in Fig. 1c. The *Green-function* and *Fourier-Kochin* patterns can be seen to be identical except near Γ where slight differences can be observed. These nearfield differences stem from the fact that the simple-singularity component $\vec{u}^S$ and the local component $\vec{u}^L$ in the flow decomposition (1) are ignored in the present implementation of the Fourier-Kochin flow representation.

Farfield extension of nonlinear nearfield steady flow about the Wigley hull

Application to the Wigley hull is now summarized. The Wigley hull is defined by

$$y = \pm b\,(1 - 4\,x^2)\,[1 - (z/d)^2] \qquad \text{with} \quad b = 0.05\ ,\ d = 0.0625$$

The nearfield flow is computed using the fully nonlinear calculation method, based on the Euler flow equations, of *Yang and Löhner (1998)*. The nearfield flow is evaluated at the matching boundary surface Σ defined by

$$x^2/a^2 + y^8/b^8 + z^8/c^8 = 1 \qquad \text{with} \quad a = 0.6\ ,\ b = 0.055\ ,\ c = 0.1 \tag{6}$$

The solution domains in the Fourier-Kochin flow representation and the nonlinear nearfield flow calculation method are respectively bounded by the mean free-surface plane $z = 0$ and the actual free surface $z = e$, where e stands for the computed free-surface elevation. The nearfield flow computed at the *Euler* matching boundary surface (with $z \leq e$) is therefore mapped onto the *Fourier-Kochin* boundary surface (with $z \leq 0$) required for the farfield flow extension. A continuous flow mapping based on linear interpolation is used here. The disturbance velocity distribution, predicted by the Euler nearfield flow solver and used in the Fourier-Kochin flow extension, at the matching boundary surface (6) is depicted in Fig. 2a for $F = 0.316$.

The nonlinear Euler nearfield wave patterns and their linear Fourier-Kochin farfield extensions are shown in Fig. 2b for $F = 0.25, 0.316$, and 0.408. The nearfield and farfield wave patterns appear to be in fairly good agreement, especially in view of the limitations inherent to both the farfield and the nearfield flows. In particular, the simple-singularity component $\vec{u}^S$ and the local component $\vec{u}^L$ in the flow decomposition (1) are ignored in the present implementation of the Fourier-Kochin flow representation, as was already noted. In addition, numerical damping attenuates the nearfield flow relatively quickly.

The *nearfield drag* predicted by the nonlinear Euler nearfield flow solver — via integration of the hull pressure — and the *farfield drag* obtained in the Fourier-Kochin extension — via the

Havelock formula (5) for the wave energy associated with the spectrum function (4) — are listed below, together with the corresponding experimental values :

F	Near	Far	Exp
0.250	0.97	0.90	0.82
0.316	1.58	1.55	1.525
0.408	2.33	2.27	2.31

The foregoing theoretical and experimental values of the wave drag coefficient (multiplied by 1000) are in relatively fair agreement.

Conclusion

The Fourier-Kochin theory of steady and time-harmonic ship waves expounded in *Noblesse et al. (1997,1999)* has been applied to *farfield steady* ship waves. This theory defines the farfield steady waves generated by a given velocity distribution $\vec{u}_g$ over a boundary surface $\Sigma \cup \Gamma$ in terms of the single Fourier integral (3) and the spectrum function (4), which is defined *explicitly* in terms of $\vec{u}_g$. The related wave drag can also be obtained *directly* from $\vec{u}_g$ and the spectrum function S, via the Havelock formula (5).

For the purpose of verifying the Fourier-Kochin representation of farfield steady ship waves, the linear free-surface potential flow due to a submerged point source of unit strength, i.e. a Green function, has been considered. Briefly, the disturbance velocity generated by the point source has been evaluated at a boundary surface Σ enclosing the source, and extended outside Σ using the Fourier-Kochin flow representation. The *outer* flow fields — outside Σ — determined *directly*, using the expressions for the gradient of the Green function given in *Ponizy et al. (1994)*, and *reconstructed* via the Fourier-Kochin theory are in agreement (Fig. 1c) as expected.

The Fourier-Kochin representation of farfield ship waves given here can be used to extend nonlinear nearfield ship waves — predicted by any nearfield flow calculation method — into the far field. An illustrative application to the Wigley hull has been presented. The nearfield flow in this example is determined using the fully nonlinear calculation method, based on the Euler flow equations, of *Yang and Löhner (1998)*. The nonlinear Euler nearfield wave patterns and their linear Fourier-Kochin farfield extensions are in fairly good agreement (Fig. 2b), especially in view of the limitations inherent to both the farfield and the nearfield flows. In particular, only the wave component $\vec{u}^W$ in the flow decomposition (1) is considered in the present implementation of the Fourier-Kochin theory. The wave drags predicted by the Euler nearfield flow solver (via hull-pressure integration) and obtained within the Fourier-Kochin extension (by means of the Havelock formula) are also in relatively fair agreement with one another, and with experiments.

References

Noblesse F.; Yang C.; Chen X.B. (1997) *Boundary-integral representation of linear free-surface potential flows*, J. Ship Research 41 pp.10-16

Noblesse F.; Chen X.B.; Yang C. (1999) *Generic Super Green functions*, Ship Technology Research 46

Ponizy B.; Noblesse F.; Ba M.; Guilbaud M. (1994) *Numerical evaluation of free-surface Green functions*, J. Ship Research 38 pp.193-202

Yang C.; Löhner R. (1998) *Fully nonlinear ship wave calculation using unstructured grid and parallel computing*, Proc. 3rd Osaka Colloquium on Advanced CFD Applications to Ship Flow and Hull Form Design, Osaka, Japan, pp.125-150

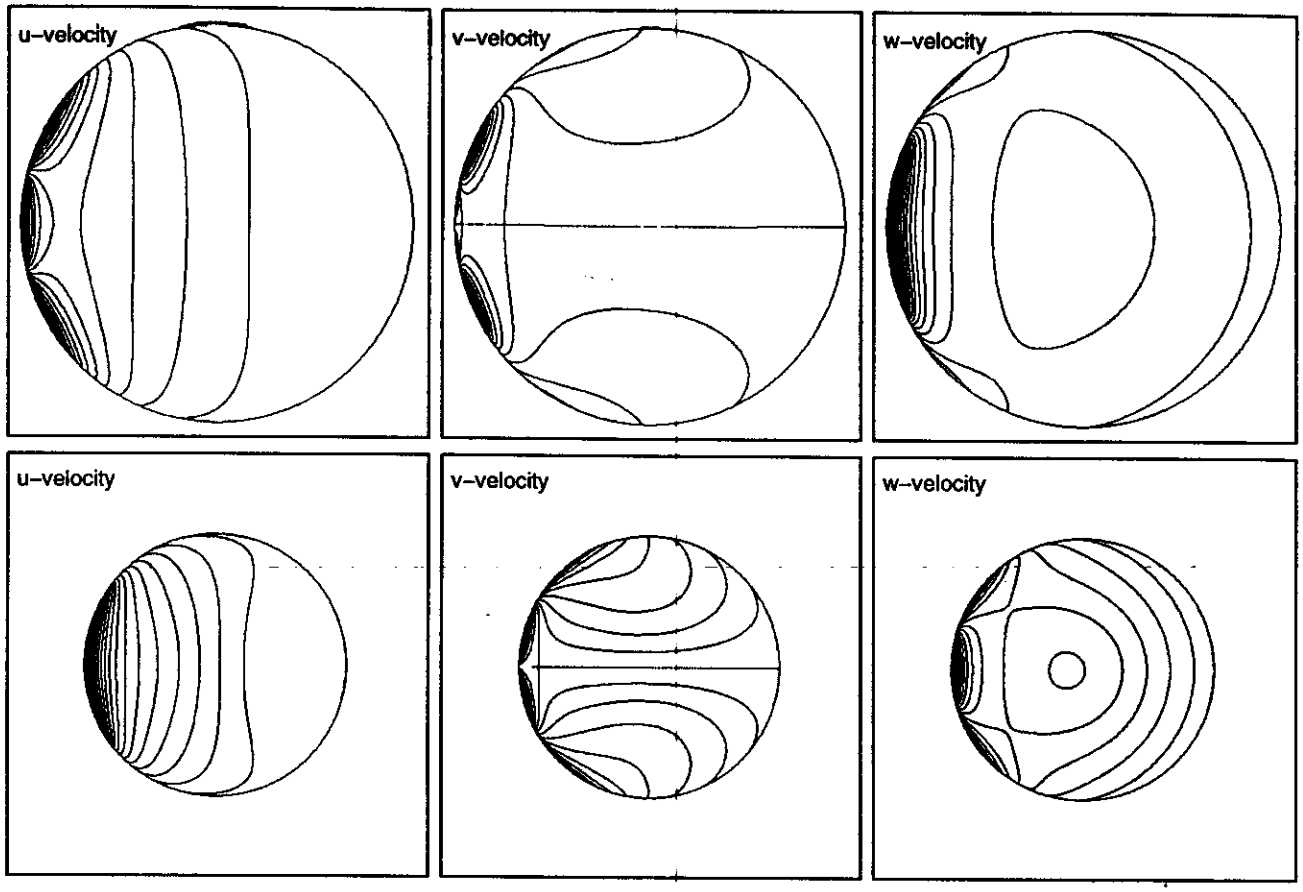

Fig. 1a. Disturbance Velocity Distribution Generated by a Point Source on Two Half Spheres

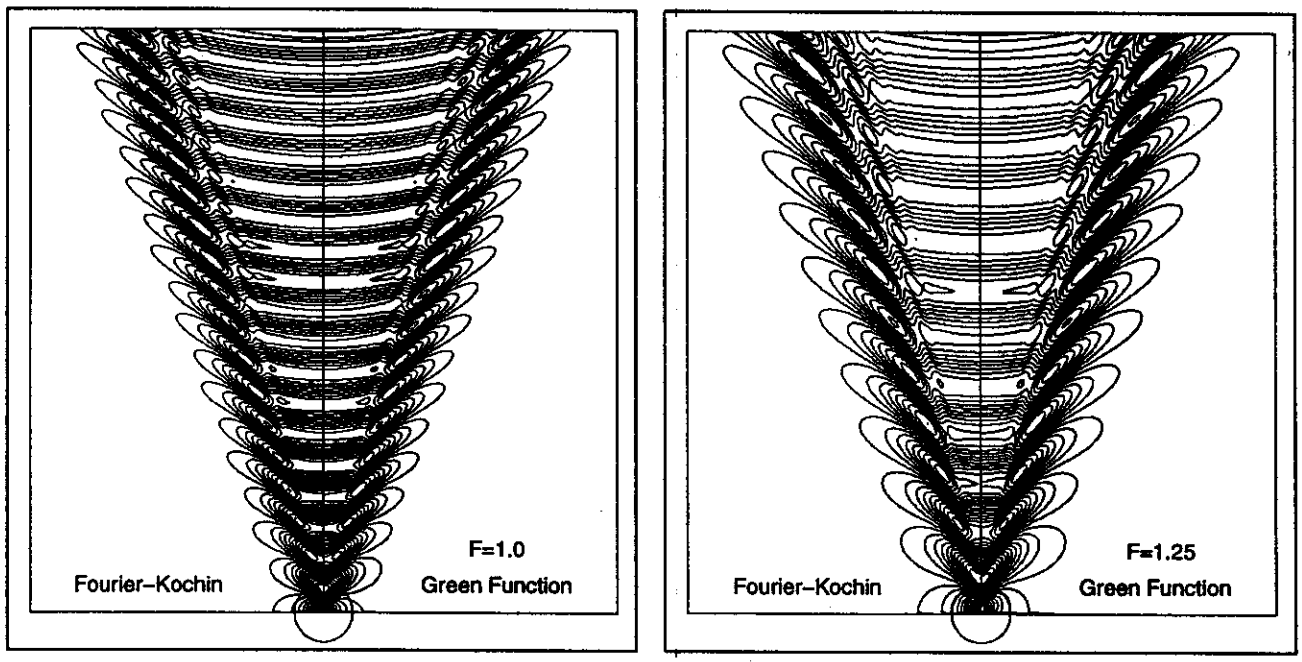

Fig. 1c. Wave Patterns Generated by a Submerged Point Source

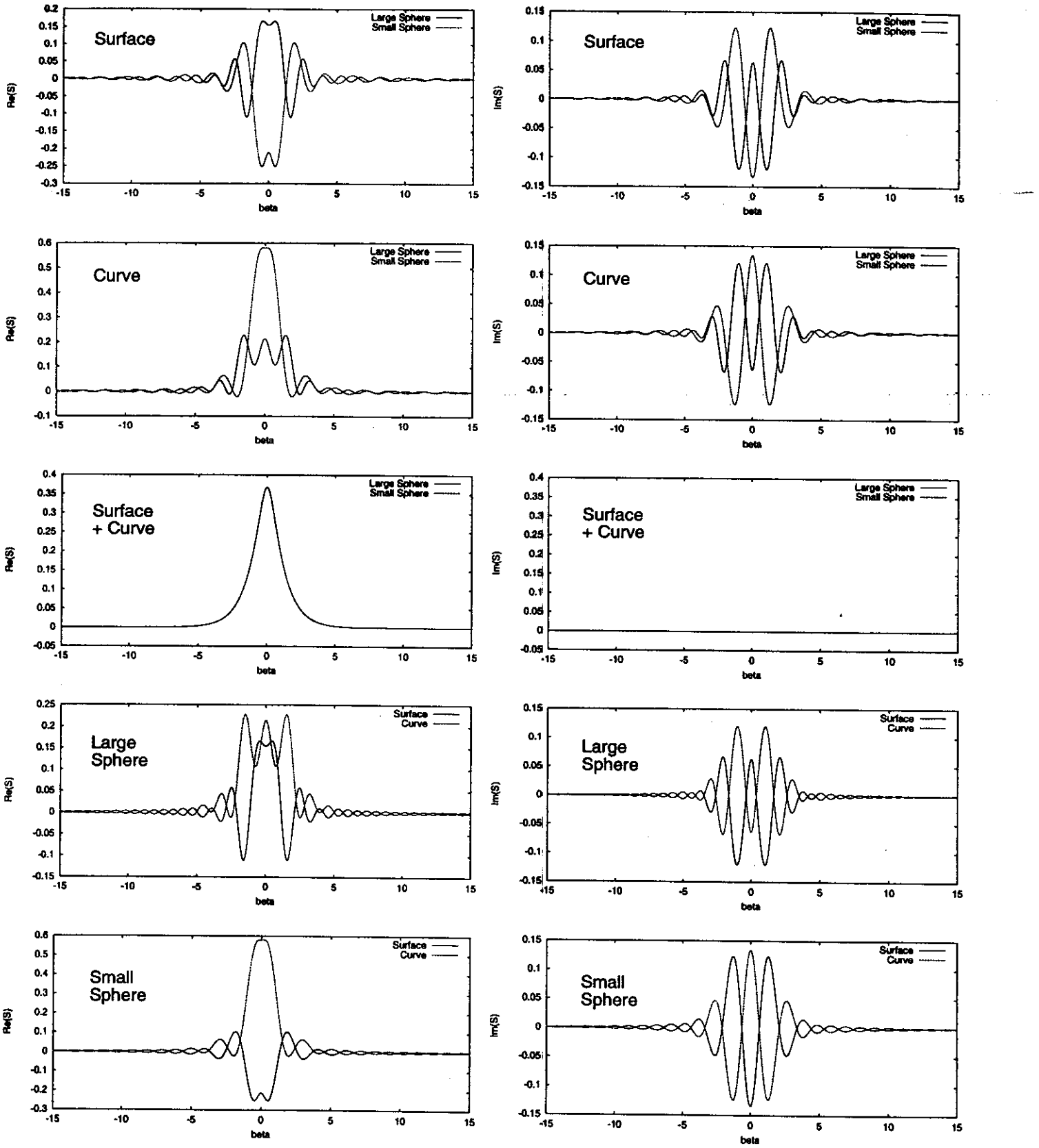

Figure 1b. Spectrum Functions Associated with Velocity Distributions on Two Half Spheres

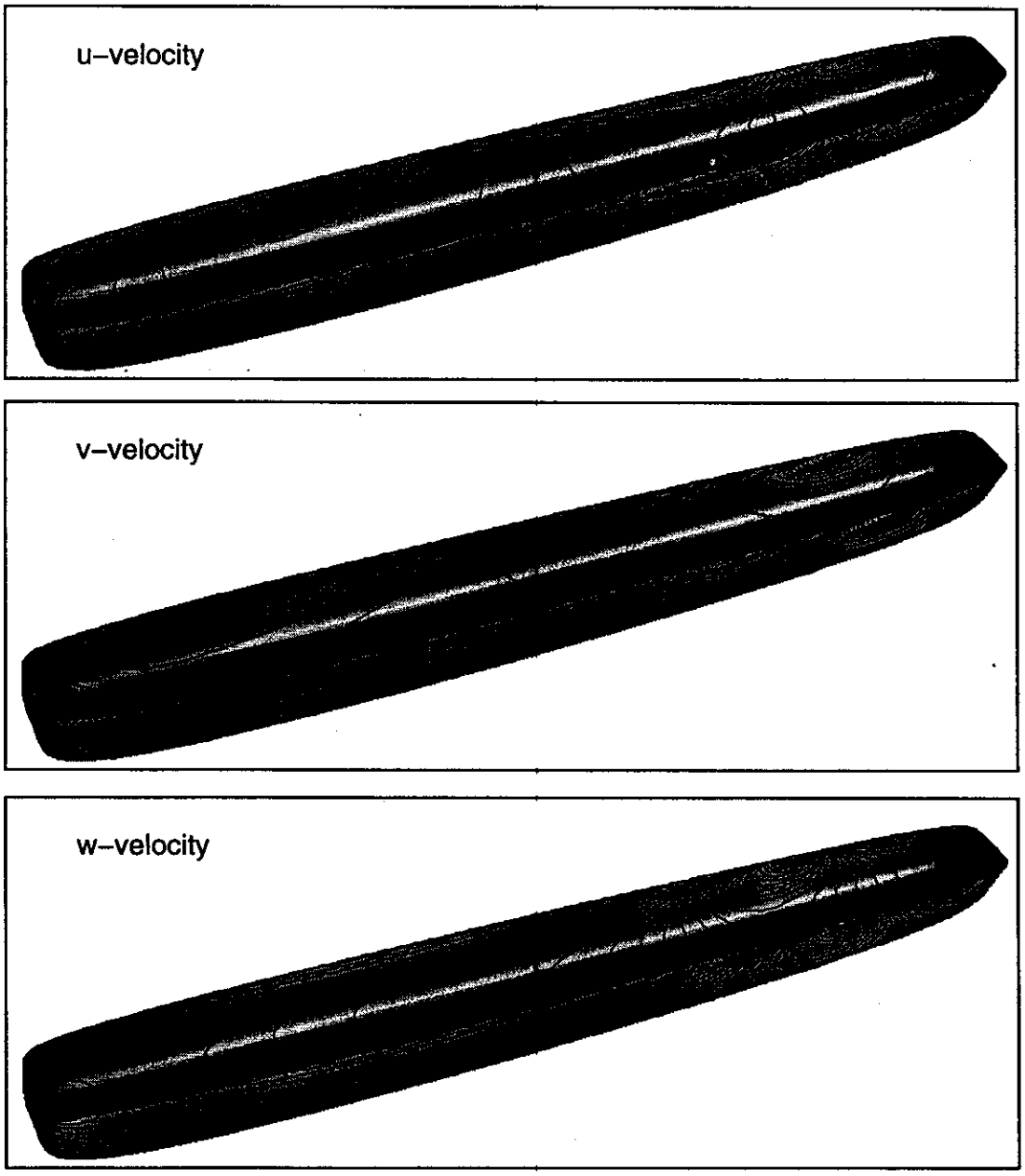

Figure 2a. Disturbance Velocity Distribution on Boundary Surface (Wigley Hull, F=0.316)

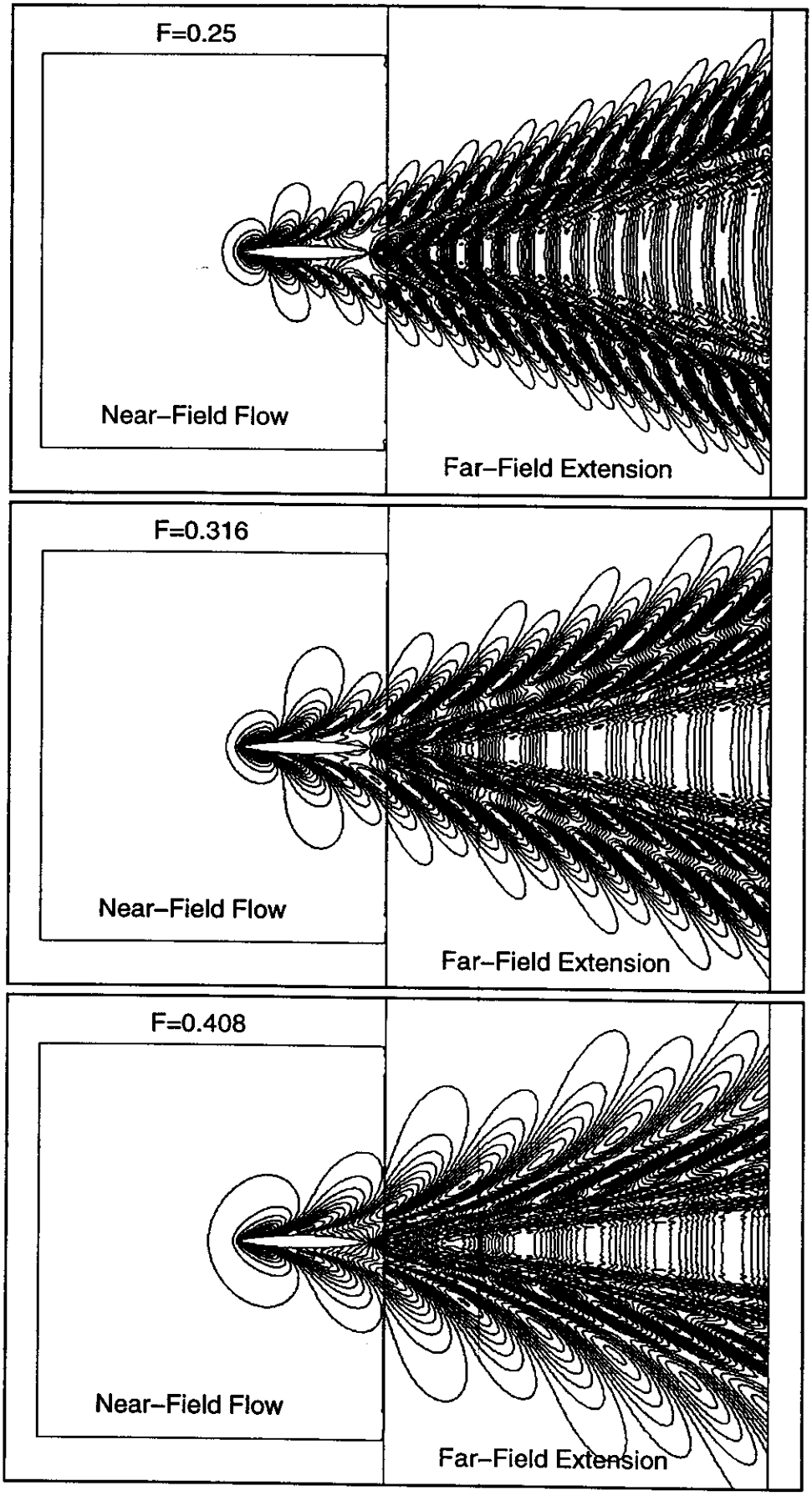

Figure 2b. Wave Patterns Generated by the Wigley Hull